

Article

Multi-Scale Analysis of Terahertz Time-Domain Spectroscopy for Inversion of Thermal Growth Oxide Thickness in Thermal Barrier Coatings

Rui Li ^{1,2,3,4,5} , Dongdong Ye ^{1,2,3,4,5,*}, Jianfei Xu ⁶ and Jiabao Pan ^{1,*} 

¹ School of Mechanical Engineering, Anhui Polytechnic University, Wuhu 241000, China; lirui1011@stu.ahpu.edu.cn

² Fujian Provincial Key Laboratory of Terahertz Functional Devices and Intelligent Sensing, Fuzhou University, Fuzhou 350108, China

³ School of Artificial Intelligence, Anhui Polytechnic University, Wuhu 241000, China

⁴ Huzhou Key Laboratory of Terahertz Integrated Circuits and Systems, Yangtze Delta Region Institute (Huzhou), University of Electronic Science and Technology of China, Huzhou 313001, China

⁵ Anhui Key Laboratory of Detection Technology and Energy Saving Devices, Anhui Polytechnic University, Wuhu 241000, China

⁶ Department of Automotive Engineering and Intelligent Manufacturing, Wanjiang College of Anhui Normal University, Wuhu 241008, China; wuhuuniversityxf@163.com

* Correspondence: ddyecust@ahpu.edu.cn (D.Y.); panjiabao@ahpu.edu.cn (J.P.)

Abstract: To address the inverse problem of thermal growth oxide (TGO) thickness in thermal barrier coatings (TBCs), a novel multi-scale analysis (MSA) method based on terahertz time-domain spectroscopy (THz-TDS) is introduced. The proposed method involves a MSA technique based on four wavelet basis functions (db4, sym3, haar, coif3). Informative feature parameters characterizing the TGO thickness were extracted by performing continuous wavelet transform (CWT) and max-pooling operations on representative wavelet coefficients. Subsequently, multi-linear regression and machine learning regression models were employed to predict and assess the wavelet feature parameters. Experimental results revealed a discernible trend in the wavelet feature parameters obtained through CWT and max-pooling in the MSA, wherein the visual representation of TGO thickness initially increases and then gradually decreases. Significant variations in these feature parameters with changes in both thickness and scale enabled the effective inversion of TGO thickness. Building upon this, multi-linear regression and machine learning regression prediction were performed using multi-scale data based on four wavelet basis functions. Partial-scale data were selected for multi-linear regression, while full-scale data were selected for machine learning regression. Both methods demonstrated high accuracy prediction performance. In particular, the haar wavelet basis function exhibited excellent predictive performance, as evidenced by regression coefficients of 0.9763 and 0.9840, further confirming the validity of MSA. Hence, this study effectively presents a feasible method for the inversion problem of TGO thickness, and the analysis confirms the promising application potential of terahertz time-domain spectroscopy's multi-scale analysis in the field of TBCs evaluation. These findings provide valuable insights for further reference.

Keywords: thermal barrier coatings; terahertz time-domain spectroscopy; multi-scale analysis; thermal growth oxide



Citation: Li, R.; Ye, D.; Xu, J.; Pan, J. Multi-Scale Analysis of Terahertz Time-Domain Spectroscopy for Inversion of Thermal Growth Oxide Thickness in Thermal Barrier Coatings. *Coatings* **2023**, *13*, 1294. <https://doi.org/10.3390/coatings13071294>

Academic Editors: Youn ho Cho, Vimalathithan Paramasamy Kannan, Claudia Barile and Young H. Kim

Received: 20 June 2023

Revised: 18 July 2023

Accepted: 21 July 2023

Published: 24 July 2023



Copyright: © 2023 by the authors. Licensee MDPI, Basel, Switzerland. This article is an open access article distributed under the terms and conditions of the Creative Commons Attribution (CC BY) license (<https://creativecommons.org/licenses/by/4.0/>).

1. Introduction

With the increasing thrust-to-weight ratio in the current aerospace field, the demands for aero-engine hot-end components have become more stringent. Aero-engine turbine inlet temperatures have already surpassed 1500 °C, presenting a challenge for conventional high-temperature alloys to meet the required safety standards [1]. To extend the service life of these components, ceramic coatings are applied to the surfaces of metallic materials,

combining the superior strength and toughness of metals with the high temperature resistance of ceramics. This enables the creation of multi-layered systems with exceptional thermal insulation properties, referred to as thermal barrier coatings (TBCs) [2]. TBCs are applied to the hot-end components of aero-engines operating in high-temperature service environments to offer thermal protection. They efficiently obstruct heat conduction, reduce surface temperatures, and enhance the material's heat resistance and service life. Typical TBCs consist of a multi-layer structure, featuring a ceramic top layer principally containing ceramic powders such as yttria-stabilized zirconia (ZrO_2 8 wt.% Y_2O_3 , 8YSZ). The ceramic layer exhibits low thermal conductivity, providing optimal thermal insulation protection. Typically, the metal bond coat layer includes MCrAlY (M represents Ni, Co, or other materials) material, which significantly improves the bonding strength between the ceramic layer and the substrate. Simultaneously, it also helps prevent oxidation and corrosion of the metal substrate. Usually, high-temperature nickel-based alloys are used as the metal substrate [3]. However, in harsh high-temperature service environments, oxygen could infiltrate the coating's pores, cracks, or interface defects and react with aluminum and other elements present in the coating, resulting in the formation of oxide compounds. These oxide layers gradually accumulate, giving rise to the formation of a thermal growth oxide (TGO) layer between the ceramic layer and the bond coat [4,5]. The main constituent of TGO is typically $\alpha\text{-Al}_2\text{O}_3$. The growth process of TGO can be broadly categorized into three stages: the rapid growth of Al_2O_3 , stable growth, and the appearance of mixed oxides accompanied by rapid thickening [6]. The formation of TGO could result in coating damage and delamination, thereby impacting the service life of the thermal barrier coating [7]. When the TGO thickness reaches a critical value of 12–15 μm , cumulative interfacial thermal mismatch stresses occur, resulting in the development of cracks in TBCs and hastening coating failure, posing a threat to the service life of TBCs. Therefore, the monitoring and evaluation of TGO thickness, as a critical aspect of TBCs, are of great importance in ensuring the functionality and lifespan of the coating [8–10].

To achieve accurate measurement of TGO thickness in TBCs, researchers have conducted extensive studies over the past few decades. Traditional methods for measuring TGO thickness include metallographic microscopy and scanning electron microscopy [11] (SEM), which involve examining electron microscope images of cross-sections of the TBCs to obtain high-resolution surface morphology and microstructural images. The impedance spectroscopy method may also be used. Huang et al. [12] utilized impedance spectra to assess TGO growth and interpreted the electrical response related to TGO thickness using an equivalent circuit model. The findings indicated that the thickness of alumina could be evaluated through the modulus spectra. The ultrasonic method is another possibility. Ma et al. [13] introduced the use of ultrasonic reflection coefficient amplitude spectra (UR-CAS) to evaluate the TGO at the interface between ceramic coating and adhesive coating in TBCs. Theoretical analysis revealed that the acoustic impedance matching between the ceramic coating and its adjacent medium influences the URCAS. This method allowed non-destructive characterization of TGO formation in TBCs, which is highly significant for practical engineering applications. X-ray methods [14], among others, have also been utilized. These classical methods provide preliminary characterization of TGO thickness and possess specific detection advantages and scopes. However, existing methods still have areas for improvement and come with certain limitations, such as the requirement for grinding and inlaying of the coating, the destructive nature of the tests, the difficulty in preparing samples, and the time-consuming nature of the process. Therefore, there is an urgent need for advanced, non-destructive testing (NDT) that overcomes the limitations of traditional methods and provides accurate, real-time, high-precision inspection of the TGO thickness of TBCs.

Currently, terahertz time-domain spectroscopy (THz-TDS) technology has shown great potential as a non-contact and high-resolution NDT method for the characterization and evaluation of microstructures of TBCs [15,16]. Overcoming the limitations of conventional methods, THz-TDS provides a superior solution. Terahertz radiation operates within

the frequency range of 0.1–10 THz, lying between microwaves and infrared waves. Terahertz waves exhibit strong penetration capabilities and high resolution, allowing detailed information on the TBC's internal structure to be obtained. Ye et al. [17–19] conducted valuable research on the NDT of the microstructure in TBCs using terahertz technology, with a focus on the porosity, interface cracks, and surface erosion damage of TBCs. This research team proposed the time-domain broadening effect to measure the porosity and applied machine learning algorithms to accurately analyze terahertz signals in time and frequency domains, promoting the development of terahertz technology in the NDT of TBCs. Chen et al. [20] proposed the use of the terahertz reflection method combined with the time-domain simulation technique for the characterization of the interfacial oxide layer. Zhang et al. [21] proposed an improved time of flight (TOF) method for measuring the TGO thickness in TBCs using terahertz time-domain spectroscopy. The method achieved efficient and accurate TGO thickness measurement, making it suitable for condition monitoring and life prediction of TBCs. Luo et al. [22] proposed a novel SWT-BP algorithm combining stationary wavelet transform (SWT) and a BP neural network for accurate thickness prediction of thin TGO in TBCs using THz-TDS. The algorithm achieved a regression coefficient of 0.92 and demonstrated good agreement with real-time results, making it suitable for detecting TGO thickness in the range of 1–29 μm . Based on previous research, effective methods can be applied to detect the thickness of TGO. By analyzing the THz-TDS, feature extraction and analysis were performed to capture and interpret information to achieve an accurate inversion of the TGO thickness. Information about the TGO layer, such as its thickness, morphology, and physical properties, could be obtained. This made THz-TDS an effective tool for the accurate inversion of TGO thickness in TBCs.

The primary objective of this study was to investigate the issue of TGO thickness inversion in TBCs. The research is of great significance as it introduces an NDT method based on multi-scale analysis (MSA) of THz-TDS, enabling real-time and accurate estimation of the TGO thickness in TBCs. In comparison to traditional methods, this approach offers distinct advantages in terms of non-destructiveness, real-time capability, and high precision, thereby facilitating effective monitoring of performance changes and lifespan assessment of TBCs. THz-TDS data were obtained through FDTD simulation, and continuous wavelet transform (CWT) was employed for MSA to extract feature parameters at various scales. Furthermore, four wavelet basis functions were compared and evaluated to determine the optimal choice for predicting the TGO thickness, thereby enhancing the accuracy and reliability of the study. Subsequently, multi-linear regression and deep extreme learning machines (DELIM) were employed to develop prediction models based on their correlation with the TGO thickness, which facilitated precise prediction and inversion of TGO thickness.

Consequently, THz-TDS technology emerges as a promising approach for non-destructive measurement of TGO thickness in TBCs, offering considerable advantages and potential applications. Its implementation could provide robust support for the design and maintenance of TBCs, while also driving advancements in related fields. The research outcomes are of paramount significance in ensuring the safe operation and enhancing the performance of TBCs, while also introducing innovative insights and methodologies for utilizing THz-TDS in material characterization and defect detection. This research paves the way for the advancement and application of TBCs.

2. Models and Methods

2.1. Finite Difference Time-Domain Simulation

To investigate the TGO thickness in TBCs, terahertz time-domain spectroscopy was employed, followed by multi-scale analysis [23,24]. The simulations were conducted using the finite difference time-domain (FDTD) module. The main purpose was to simulate the propagation behavior of terahertz waves in TBCs, as shown in Figure 1, which illustrates a schematic diagram for terahertz detection of TBCs. Terahertz time-domain data related to TGO thickness were obtained, as shown in Figure 2. Specific simulation parameters were

set according to Table 1, encompassing 30 sets of different simulation data, covering a TGO thickness range of 1.000–22.609 μm .

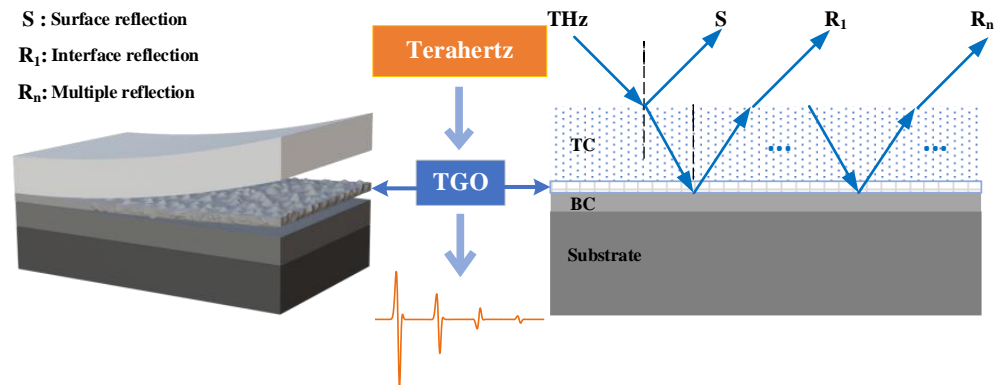


Figure 1. Schematic diagram of terahertz non-destructive testing of TBCs.

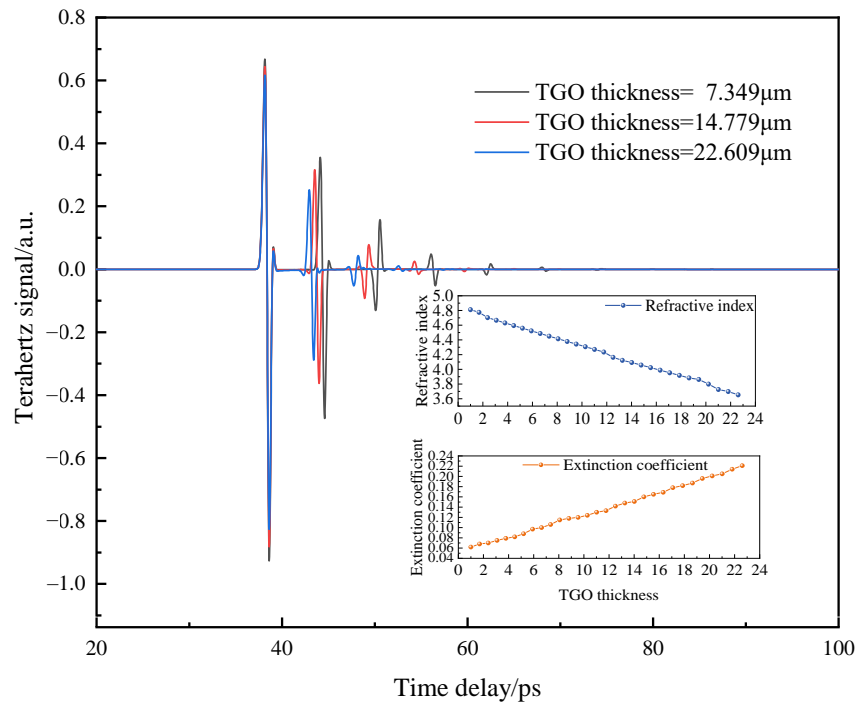


Figure 2. Terahertz time-domain signal.

Table 1. FDTD simulation parameter settings.

Parameter	Setting Conditions
Simulation time	100 ps
THz frequency	0.3–1.0 THz
TGO thickness	1.000–22.609 μm
Refractive index	3.653–4.811
Extinction coefficient	0.062–0.221
Porosity	6.220%–22.894%

The simulation parameters utilized in this study were derived from actual experimental data, demonstrating a practical foundation for the parameter settings. These parameters were systematically adjusted and planned to accommodate the specific requirements of the research focus in this study. Subsequently, these carefully selected parameters were incorporated into the FDTD module to facilitate the simulation process for terahertz detection

of TGO thickness. The simulation parameters were not arbitrarily chosen but were based on real experimental measurements. Their rational adjustment and integration into the simulation software allowed an effective and targeted investigation of terahertz detection of TGO thickness in alignment with the research objectives of this study. To make the simulation more realistic, the porosity range was set between 6.220% and 22.894%. For the FDTD simulation, the corresponding parameter settings for refractive index and extinction coefficient ranged from 3.653 to 4.811 and from 0.062 to 0.221, respectively. These settings aimed to better reflect the changes in TBCs during thermal cycling, where porosity increased and TGO thickness grew simultaneously. By varying the TGO thickness, 30 groups of THz-TDS data were generated, providing the foundation for subsequent multi-scale analysis.

TGO thickness in TBCs has a significant impact on their performance and lifespan. Typically, when the TGO thickness exceeds 15 μm , issues such as cracking and delamination are prone to occur, thereby affecting the TBC's service life. Therefore, accurate detection of the TGO thickness is crucial for assessing the health status of the thermal barrier coating.

2.2. Multi-Scale Analysis

THz-TDS is an extremely effective method for measuring TGO thickness in TBCs. By emitting and receiving terahertz electromagnetic waves and analyzing the sample's scattering, absorption, and transmission processes, complex signals containing information about the TGO can be extracted. However, due to the complexity and diversity of the TGO itself, these signals are often highly nonlinear and subject to noise interference, necessitating data processing and signal analysis to extract valuable information.

Multi-scale analysis (MSA) is a technique that involves decomposing and analyzing signals at different scales, allowing the extraction of both local and global features [25,26]. In the context of THz-TDS, applying MSA enables the transformation of terahertz signals across various scales, thereby capturing information related to different scales. In this study, continuous wavelet transform (CWT) was utilized for MSA. CWT convolved the signal with a set of wavelet functions of different scales, allowing the representation of the terahertz time-domain data as wavelet coefficients and approximation coefficients at different scales and frequencies [27]. Each layer of wavelet coefficients represented the signal's response at a specific scale and frequency domain, while the approximation coefficients represented the dominant low-frequency information. The wavelet coefficients across different layers were independent and exhibited distinct time-frequency features.

Wavelet basis functions were typically selected based on the features of signals and application requirements. As shown in Figure 3, the wavelet basis functions used in this study included Daubechies (db), Symlets (sym), Haar (haar), and Coiflets (coif). The absolute value operation was performed on the wavelet coefficients of each scale, and its maximum value was extracted, which is known as max-pooling [28]. For each scale, this process compressed the wavelet coefficients into a single scalar. Subsequently, the feature values were combined into a feature vector, with each element representing the absolute value of the maximum continuous CWT coefficient at that particular scale. The units of each feature vector element were dimensionless and the values on the vertical axis represented only relative sizes, indicating the strength of the CWT coefficient at each scale. The inversion of TGO thickness was achieved through the MSA method.

CWT was one of the essential steps in the MSA. The formula for continuous wavelet transform was as follows:

$$cwt_D(a, b) = \frac{1}{\sqrt{|a|}} \int_{-\infty}^{\infty} x(t) \psi\left(\frac{a-t}{a}\right) dt \quad (1)$$

where $cwt_D(a, b)$ is the wavelet coefficient at scale a and displacement b , $x(t)$ is the time-domain signal being analyzed, and ψ is the wavelet basis function. Processed by continuous wavelet transform, the original time-series signal could be transformed into wavelet coefficients at different scales, thereby extracting features within different time ranges.

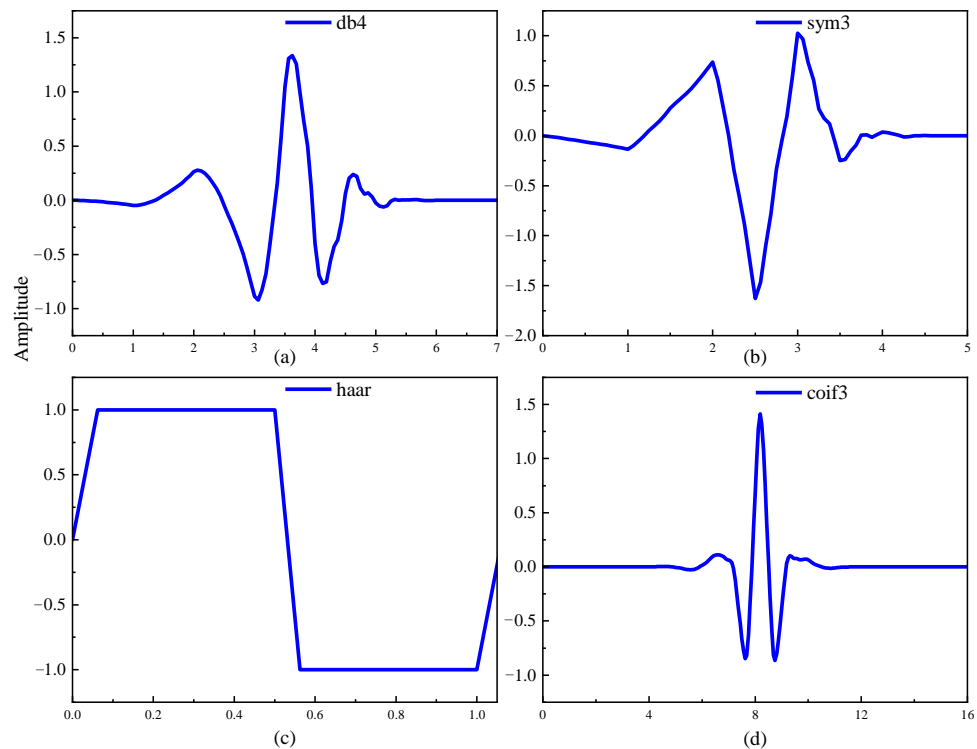


Figure 3. Wavelet basis function (a) db4, (b) sym3, (c) haar, (d) coif3.

The basic process, as shown in Figure 4, involved taking the absolute values of the wavelet coefficients at each scale and performing max-pooling. Specifically, a sliding pooling window moved with a fixed stride from left to right and top to bottom, covering the entire matrix of wavelet coefficients. The maximum value within each local window was selected, resulting in one max-pooled value for each scale. These pooled values served as the primary feature representation of the wavelet coefficients at different scales. This process reduces dimensionality and extracts the most significant feature information, highlighting the strongest variations in the wavelet coefficients while discarding weaker portions, thereby reducing redundant information. It provides more compact and critical features for further modeling and analysis.

$$f_i = \max_j |c_{i,j}|, \quad i = 1, 2, 3, 4 \quad (2)$$

$$f = (f_1, f_2, f_3, f_4) \quad (3)$$

where $c_{i,j}$ is the j -th element of the i -layer wavelet coefficient, and f_i represents the maximum response of the i -layer wavelet coefficient. This operation is equivalent to taking the absolute value of each row of data, and then taking the maximum value in the second dimension, and the obtained vector f is the eigenvector of the wavelet of the time series signal.

The feature vectors for each TGO thickness are stored. Once the wavelet feature vectors are extracted for all TGO thicknesses, further analysis can be performed.

$$features_i = f, \quad i = 1, 2, \dots, length(TGOth) \quad (4)$$

where $features_i$ denotes the feature vector at the i -th TGO thickness.

Through this method, the original time-domain signal was transformed into a fixed-length feature vector, thereby simplifying subsequent tasks such as model training, feature selection, and classification recognition. Moreover, the MSA allowed the retention of signal features at different scales and showed good interpretability and robustness.

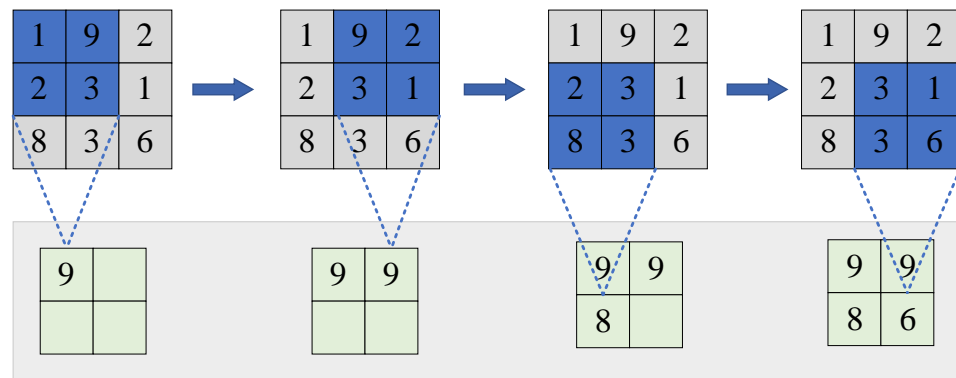


Figure 4. Structure diagram of max-pooling. The gray part is the local window of each step. The blue part is the sliding window for each step. The green part is the max-pooled value for each sliding window.

2.3. Multi-Linear Regression

Multi-linear regression is a statistical model used for elucidating the linear relationship between feature parameters and a target variable. It is applicable for investigating the relationships among two or more variables. Within the framework of multi-linear regression, there exist multiple independent variables and one dependent variable [29]. The model can be used to describe the extent to which the independent variables impact the dependent variable and predict future values of the dependent variable. In this study, multi-linear regression was implemented to examine the relationship between TGO thickness and the feature vectors of each wavelet function obtained from the wavelet decomposition of THz time-domain data. Specifically, a multi-linear regression model was constructed using the feature vectors of the wavelet functions as independent variables and TGO thickness as the dependent variable. The model was used to determine the degree of influence of each wavelet function’s feature vector on TGO thickness and to make predictions about future TGO thickness values. MSA was conducted using four different wavelet basis functions to extract wavelet feature parameters. These parameters were incorporated into the multi-linear regression model to evaluate the effectiveness of various wavelet functions in predicting TGO thickness and to identify the most effective wavelet basis function for multi-linear regression.

The following are the steps for predicting multi-linear regression:
 Normalize the data and scale it to the range of [0, 1].

$$x' = \frac{x - \min(X)}{\max(X) - \min(X)} \tag{5}$$

where x' is the normalized value, x is the original value, and X is the vector or matrix of the feature parameter.

Multi-linear regression models were used to model the linear relationship between several independent variables (wavelet feature parameters) and one dependent variable (TGO thickness). Assuming there are N sample data, in which the i -th sample’s wavelet feature parameter is expressed as $x(i)$, and the corresponding TGO thickness is expressed as $Y(i)$, where $i = 1, 2, \dots, N$.

$$Y = \beta_0 + \beta_1 X_1 + \beta_2 X_2 + \dots + \beta_p X_p + \varepsilon \tag{6}$$

where Y is the TGO thickness, X_1, X_2, \dots, X_p are wavelet feature parameters, $\beta_0, \beta_1, \dots, \beta_p$ is the regression coefficient, and ε is the error term.

Represent feature parameters and TGO thickness in matrix form:

$$Y = X\beta + \varepsilon \tag{7}$$

where Y is an $N \times 1$ -dimensional thickness matrix, X is an $N \times (p + 1)$ -dimensional matrix of feature parameters, and β is a $(p + 1) \times 1$ -dimensional vector of regression coefficients.

For the fitting of the multi-linear regression model, the estimated value of regression coefficient $\hat{\beta}$ is solved by the least square method, which minimizes the residual sum of squares:

$$\hat{\beta} = (X^T X)^{-1} X^T Y \quad (8)$$

Using the multi-linear regression model obtained from training, predictions were made on the test set to obtain the predicted values \hat{Y} .

To evaluate the performance of the multi-linear regression model, root mean square error (RMSE), mean absolute error (MAE), mean absolute percentage error (MAPE), and the regression coefficient (R^2) are commonly used as metrics:

$$MAE = \frac{1}{N} \sum_{i=1}^N |\hat{Y}_i - Y_i| \quad (9)$$

$$RMSE = \sqrt{\frac{1}{N} \sum_{i=1}^N (\hat{Y}_i - Y_i)^2} \quad (10)$$

$$MAPE = \frac{1}{N} \sum_{i=1}^N \frac{|\hat{Y}_i - Y_i|}{Y_i} \times 100\% \quad (11)$$

$$R^2 = 1 - \frac{\sum_{i=1}^N (\hat{Y}_i - Y_i)^2}{\sum_{i=1}^N (Y_i - \bar{Y})^2} \quad (12)$$

where \hat{Y}_i is the predicted value, Y_i is the test value, and \bar{Y} is the average value.

To summarize, the multi-linear regression method established a model using the wavelet feature vectors extracted from THz time-domain data and the corresponding TGO thickness as the independent and dependent variables, respectively. This method allowed the prediction of TGO thickness and the selection of the optimal wavelet function for MSA by comparing the prediction accuracy of different wavelet basis functions. By following these steps, a multi-linear regression model could be established and used for prediction, performance evaluation, and visualization of results. Through the comparison of evaluation indicators and error items, the best wavelet basis function could be determined to achieve the inversion of TGO thickness in TBCs via multi-scale analysis of THz-TDS.

2.4. Deep Extreme Learning Machine

Extreme learning machine (ELM) is a type of single-hidden-layer feedforward neural network that achieves an optimal solution by randomly generating weights and thresholds. However, due to its simple architecture, an ELM cannot effectively capture deep hierarchical relationships. Therefore, the deep extreme learning machine (DELIM) was introduced to explore deep relationships [30,31].

As shown in Figure 5, DELIM is a multi-layer neural network composed of an extreme learning machine as autoencoder (ELM-AE), an unsupervised learning algorithm used to extract effective feature information by copying input information to output data through training. Compared with traditional algorithms, each hidden layer's input weight in DELIM was initialized using ELM-AE and underwent hierarchical unsupervised training. Assuming k nodes for the input and output layers and l nodes for the hidden layer, ELM-AE achieved feature mapping of equal dimensions when $k = l$, dimensionality reduction feature mapping when $k > l$, and high-dimensional feature mapping when $k < l$.

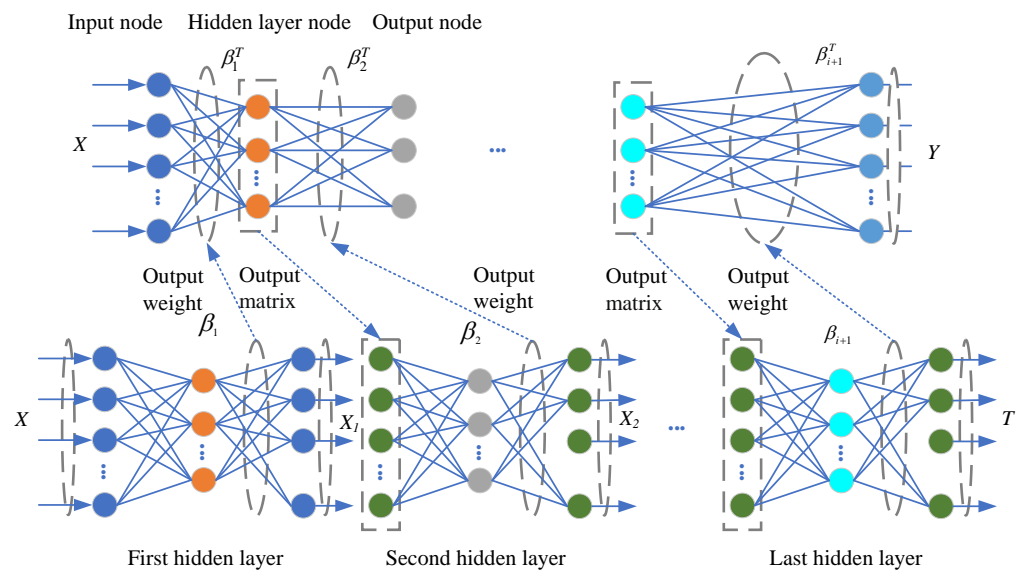


Figure 5. Structure diagram of DELM.

Equidimensional feature mapping, implicit layer input weight matrix β :

$$\beta = H^{-1}T \tag{13}$$

where H is the hidden layer output matrix and T is the target output matrix.

High and low dimensional feature mapping, implicit layer input weight matrix β :

$$\beta = \left(\frac{E}{\mu} H^T H \right)^{-1} H^T X \tag{14}$$

where E is the identity matrix, X is the input matrix, and μ is the regularization coefficient.

DELM offered a more comprehensive exploration of the mapping relationships among data, enhancing non-linear fitting capability and predictive performance. Moreover, DELM eliminates the need for backpropagation, rendering the network’s training time significantly shorter. During DELM training, the original input samples were employed as the target output matrix for the initial ELM-AE, leading to the derivation of an output weight matrix. This weight matrix was subsequently orthogonalized and utilized as the input weight matrix for the first hidden layer within DELM. The output of the first hidden layer served as the input matrix of the subsequent ELM-AE, and this process continued layer by layer until the last layer’s output weight matrix was obtained, thus completing the training process of DELM.

DELM is an advanced deep learning algorithm renowned for its quick training process and outstanding performance, making it well suited for feature extraction and regression prediction tasks on extensive datasets. For TGO thickness prediction, the wavelet feature parameters obtained through wavelet analysis were used as the input layer’s feature vectors, while TGO thickness was considered as the output layer’s dependent variable. The DELM algorithm was applied to train the model and predict the TGO thickness of unknown samples. The selection of the optimal wavelet function was achieved by comparing the prediction accuracy across different wavelet basis functions. A specific methodology involved partitioning the dataset into training and testing sets with a certain ratio. The DELM algorithm was then utilized to train the model using the training set, and subsequent predictions were made on the testing set. Error indicators, such as those discussed in Section 2.3, were computed to evaluate the prediction accuracy and enable comparison across different wavelet basis functions.

3. Results and Discussion

3.1. Continuous Wavelet Transform

Continuous wavelet transform (CWT) is a signal analysis method based on scale transformation, which effectively captures the local features of a signal in both the time and frequency domains. CWT was used to characterize the TGO thickness in TBCs by decomposing and reconstructing the signal using wavelet basis functions. TGO thickness gradually increased as the TBCs were exposed to service time. When a terahertz signal traversed the TBCs, it experienced an influence from the TGO thickness, resulting in changes in the numerical values of the wavelet coefficients. Therefore, by employing CWT to process the time-domain signal and extracting parameters from the wavelet matrix to represent the degree of signal variations, the relationship between TGO thickness and terahertz signal could be revealed.

The four wavelet basis functions used in this study were db4, sym3, haar, and coif3. CWT operated by convolving these basis functions with the signal, which was translated and scaled in the time and scale dimensions. This process enabled the decomposition of the signal on the time-scale plane, yielding continuous wavelet coefficients that provided insights into the time-varying properties and energy distribution of the signal across different scales and frequencies.

Specifically, each set of THz-TDS data corresponding to TGO thickness had a dimension of 3700, with 30 sets of data in total. Taking db4 as an example of the wavelet basis function, a scale value of 50 was selected. The original THz data underwent CWT resulting in a dimension of 50×3700 . Each time series point was analyzed across 50 scales to obtain 50 coefficient sequences, with each value representing the relative strength of the signal at that scale. Each column consisted of 50 numerical values, representing the wavelet coefficients at the corresponding scale. As shown in Figure 6, the data of 50-scale analyses for the time series extracted from the 400th, 900th, 1300th, 1700th, 2100th, 2500th, 2900th, 3300th, and 3700th columns were used to represent the energy distribution at different scales at corresponding time points. Thus, it could be observed that the wavelet coefficients of THz-TDS signals exhibited complex variations and redundant characteristics across different scales. To extract the key features of the signal and reduce redundancy, max-pooling was applied to the wavelet coefficient matrix.

3.2. The Result of Max-Pooling

Max-pooling, a prevalent technique for feature extraction, reduces the dimensionality of a feature matrix by choosing the maximum value within each local region. Specifically, for each time point (each column), max-pooling selected the element with the maximum value from the corresponding wavelet coefficients, obtaining the maximum response of the wavelet coefficients at that scale. This formed a new feature vector, where each element was a dimensionless scalar representing the absolute value of the maximum continuous wavelet transform coefficient at the corresponding scale. These features reflected the maximum degree of variation in the signal at different scales.

By further processing these wavelet coefficients, the most significant information related to the signal's features could be extracted. In this study, the max-pooling method was employed to extract features, whereby the maximum wavelet coefficient at each scale was selected as the feature value, transforming the results of multi-scale analysis into a fixed-length feature vector representation.

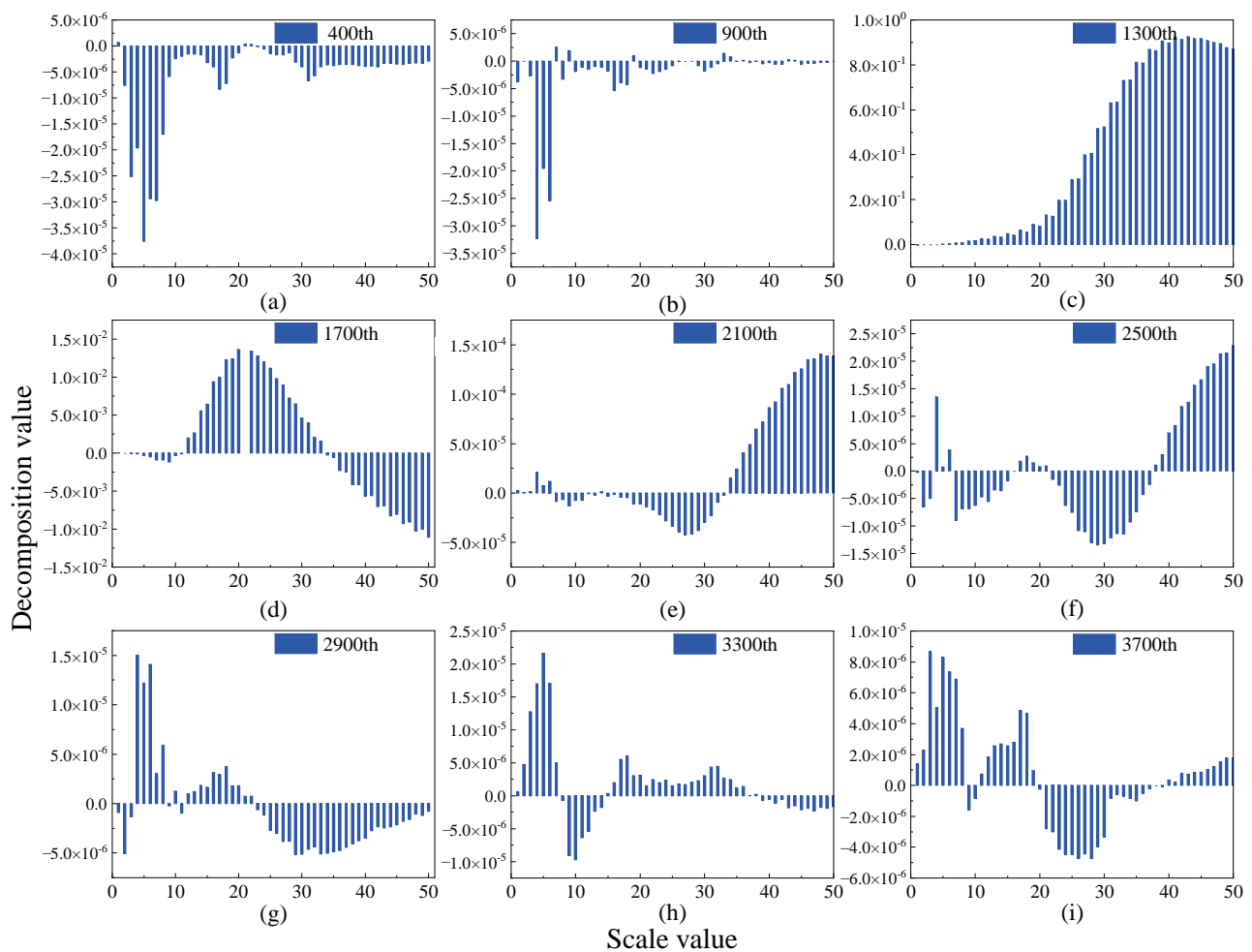


Figure 6. 50-scale decomposition for each time series point: (a) 400th, (b) 900th, (c) 1300th, (d) 1700th, (e) 2100th, (f) 2500th, (g) 2900th, (h) 3300th, (i) 3700th.

As shown in Figure 7, it was evident that through the process of max-pooling, the complexity and redundancy of the wavelet coefficients were further reduced, resulting in more regular feature curves. The extrema of the feature curves corresponding to the four wavelet bases occurred at the 33th, 32th, 38th, and 34th scales, respectively, exhibiting a descending trend after reaching the extremum points. The pattern of the feature curve, initially increasing and then decreasing, was attributed to the combination of filters used in wavelet decomposition, which smoothed the signal to different extents and extracted details at various scales. The wavelet coefficients at smaller scales primarily captured the signal's detailed information, while those at larger scales reflected its overall characteristics. Initially, as the scale increased, the feature parameters gradually increased. This was attributed to the smaller scales' ability to capture high-frequency details and local variations in the terahertz signal, which might be correlated with the TGO thickness. However, as the scale further increased, the feature parameters reached a peak and gradually decreased. Because larger scales captured low-frequency global features in terahertz signals, the correlation between these features and TGO thickness may have been weak. Therefore, at larger scales, the characteristic parameters gradually decreased.

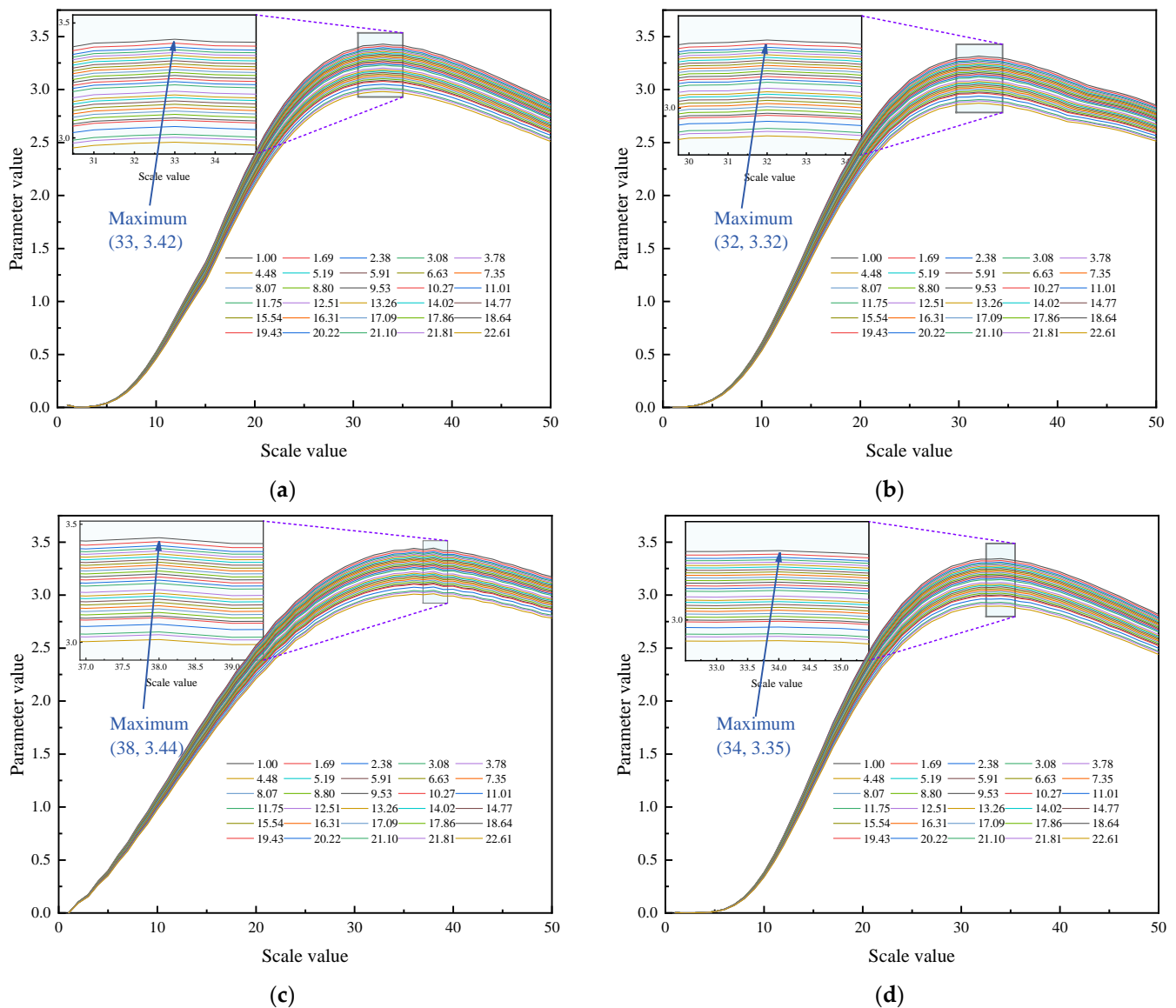


Figure 7. Multi-scale features of max-pooling processing: (a) db4, (b) sym3, (c) haar, (d) coif3.

To further validate the accurate representation ability of the feature parameters extracted through multi-scale analysis for TGO thickness, multi-linear regression and machine learning regression were chosen as additional prediction methods. These methods allowed modeling and prediction of the relationship between the feature parameters obtained from MSA and TGO thickness, thereby enabling a more effective evaluation and comparison of the predictive accuracy of MSA data employing distinct wavelet basis functions.

3.3. Performance Evaluation of Multi-Scale Analysis

This section mainly introduces the use of feature parameters obtained through MSA based on four wavelet functions as independent variables for predicting TGO thickness using multi-linear and machine learning regression models. The performance of MSA was evaluated and compared using metrics such as MAE, RMSE, MAPE, and R^2 .

For multi-linear regression, considering the rank deficiency of the regression design matrix, based on the analysis of wavelet coefficients in Section 3.2, scales around the peak were selected as representative features. This selection was justified as scales in the vicinity of peaks often encapsulate the most salient information pertaining to variations in TGO thickness, thus significantly contributing to TGO thickness prediction. By selecting a

subset of scales as independent variables, the dimensionality was reduced while ensuring the nonsingularity of the regression design matrix and avoiding rank deficiency issues. Specifically, scales 21 to 40 for each of the 30 thicknesses were chosen as the independent variables for the multivariate regression to ensure the nonsingularity of the design matrix. As shown in Figure 8, the multi-linear regression predictions were presented for the four wavelet basis functions, with the haar wavelet exhibiting the highest degree of conformity with the test values. Table 2 displays the results of various evaluation metrics, indicating that the R^2 values for haar, coif3, sym3, and db4 were 0.9763, 0.9093, 0.8944, and 0.7507, respectively.

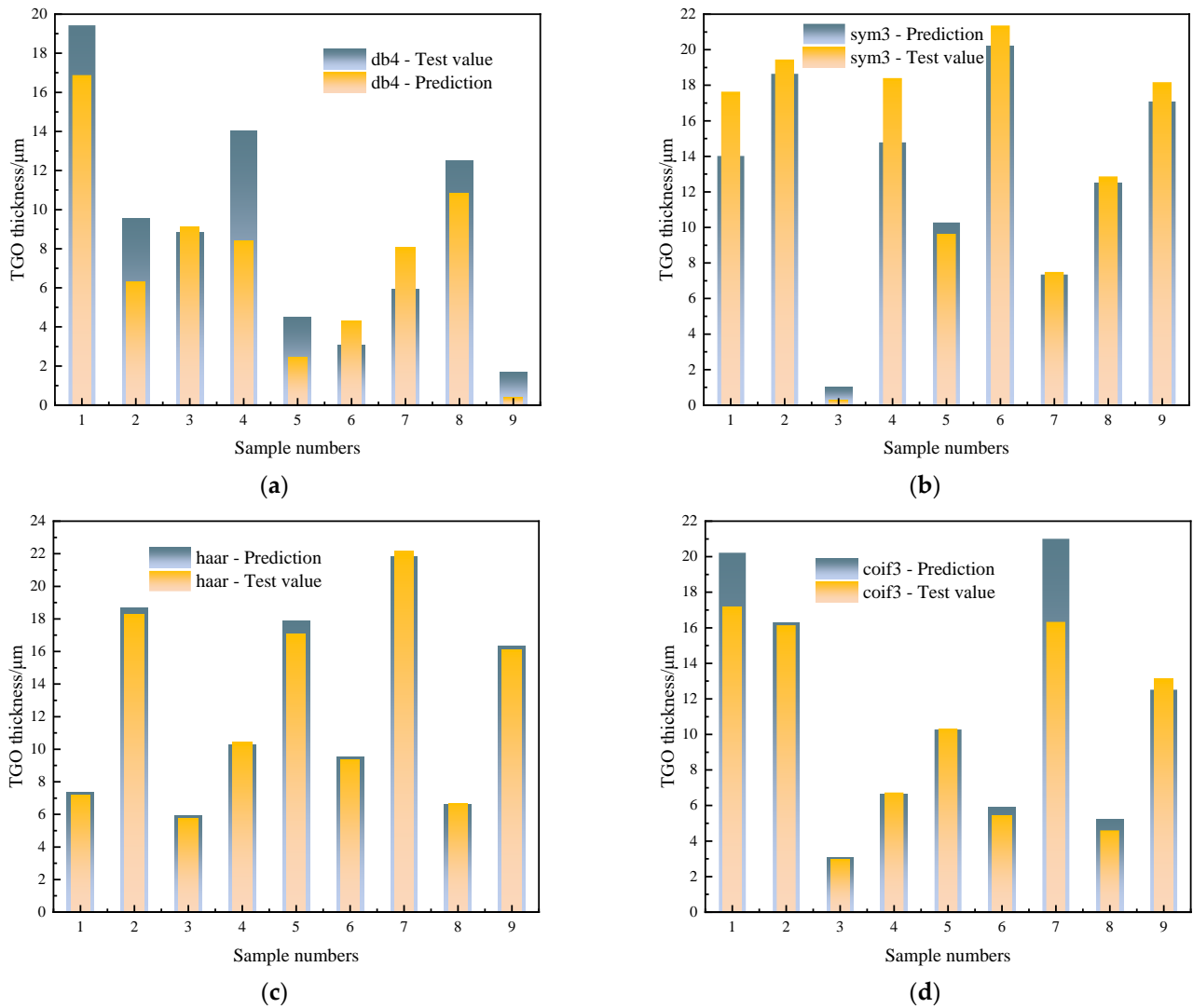


Figure 8. Multi-linear regression prediction results: (a) db4, (b) sym3, (c) haar, (d) coif3.

Table 2. Multi-linear regression evaluation index.

Types of Wavelets	MAE	RMSE	MAPE/%	R^2
db4	2.225	2.7078	26.59	0.7507
sym3	1.3483	1.8391	36.65	0.8944
haar	0.2711	0.3408	2.10	0.9763
coif3	1.1027	1.8790	9.03	0.9093

In Figure 9, the absolute error comparison diagram for multi-linear regression predictions using the feature parameters obtained from the MSA with four wavelet functions is

presented. It is evident that the haar wavelet exhibited the smallest absolute error, followed by the coif3 wavelet, sym3 wavelet, and db4 wavelet, which had the largest absolute error. However, in general, the prediction accuracy was high, with absolute errors controlled within 5.

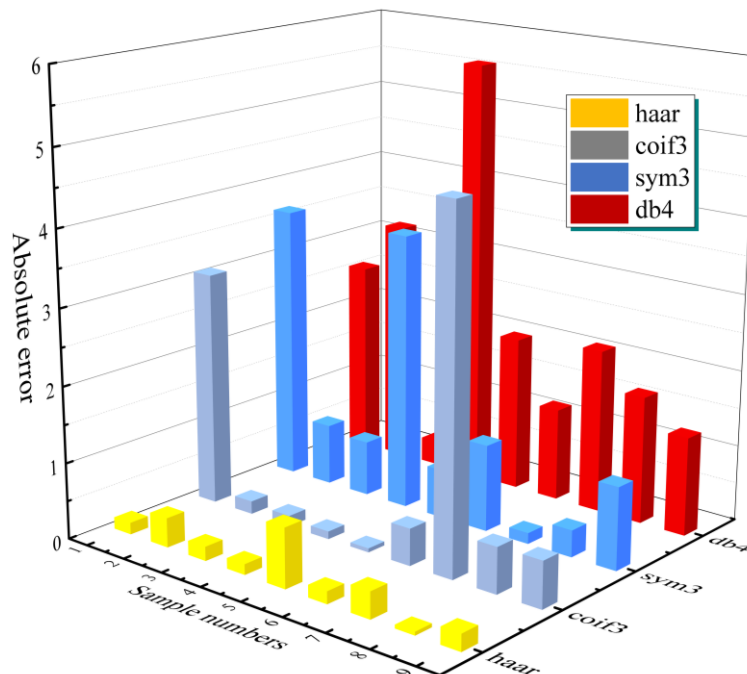


Figure 9. Absolute error comparison of prediction by multi-linear regression.

These results further validate the effectiveness of the wavelet feature parameters extracted through MSA as independent variables for linear regression prediction which can accurately invert TGO thickness, and the performance differences of different wavelet basis functions are also verified. Moreover, the higher accuracy of regression prediction achieved by the haar wavelet suggests its superior capability for feature extraction, making it a favorable choice for practical applications. This finding holds significant importance.

However, it should be noted that the multi-linear regression model was a prediction method based on linear assumptions, and its predictive capability may be limited by the assumptions of the model. In addition to evaluation metrics, the robustness, generalizability, and stability of the model were also important factors to consider. Furthermore, the quantity and quality of the samples were crucial factors that affected the predictive ability, so it was necessary to ensure an adequate and representative sample size. The results presented above demonstrate that selecting specific ranges of scale data could effectively predict the TGO thickness. Then, in order to further validate the effectiveness of the complete scale data, another set of experiments was conducted using the full 50 scales as inputs for deep extreme learning machine prediction.

In Figure 10, the machine learning regression predictions using the four different wavelet basis functions are presented. Due to the deep extreme learning machine's ability to explore the mapping relationships between variables, the predictions based on the MSA data of the four functions outperformed those of the multi-linear regression predictions. The experimental results indicate that even when using the full-scale data as input, the haar wavelet basis function still outperformed the other wavelet basis functions in terms of prediction accuracy. The discrepancy in the predicted results could be attributed to the inherent characteristics and limitations of each wavelet basis function, which affected their predictive accuracy. As shown in Figure 7, the scales corresponding to the maximum values in the wavelet decompositions were 33, 32, and 34 for db4, sym3, and coif3, respectively, while the scale for haar was 38. The multi-scale decomposition using the haar wavelet

basis function more effectively captured the variations in TGO thickness, leading to higher predictive accuracy. The haar wavelet is characterized by a step-like shape, with one positive and one negative step. It is known for its ability to detect abrupt changes in signals. The haar wavelet basis function had good temporal localization characteristics, which could accurately capture subtle features of TGO thickness changes. Considering the full-scale data, each scale contained information that was sensitive to TGO thickness to a certain degree, and the haar wavelet basis function could better extract and represent this information.

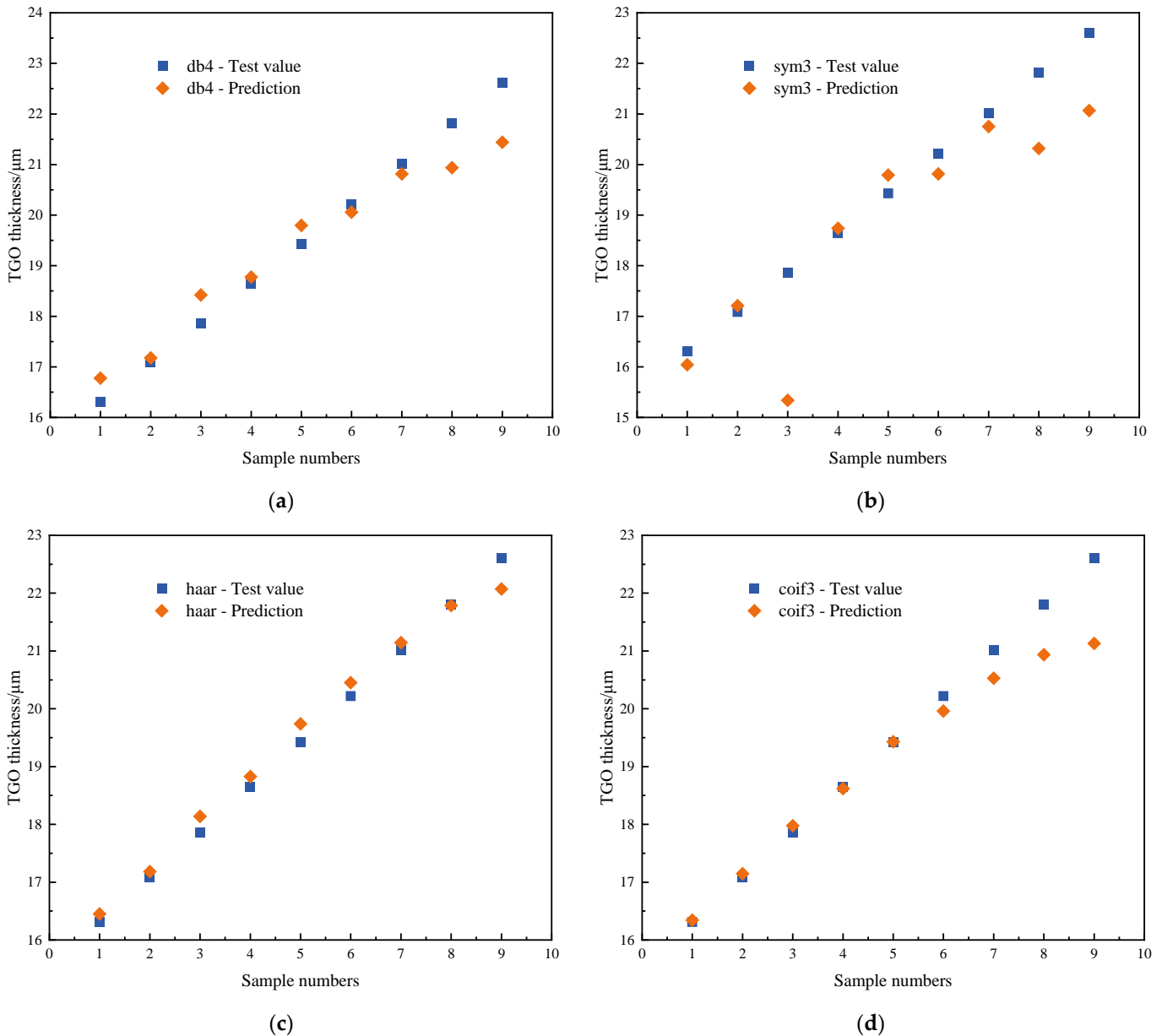


Figure 10. DELM prediction results (a) db4, (b) sym3, (c) haar, (d) coif3.

As shown in Table 3, four indices were used to evaluate the predictive performance of the deep extreme learning machine, and also to evaluate the effect of full-scale data on the thickness inversion of TGO. The R^2 of haar, coif3, db4, and sym3 were 0.9840, 0.9121, 0.9027, and 0.7921, respectively.

Figure 11 shows the prediction absolute error comparison diagram of machine learning regression for the characteristic parameters of four wavelet basis functions after processing in MSA. It could be seen that the absolute error of the haar wavelet was the smallest,

followed by the *coif3* wavelet, *db4* wavelet, and *sym3* wavelet. In general, the prediction accuracy was very high, and the absolute error was controlled within 2.5.

Table 3. DELM regression evaluation index.

Types of Wavelets	MAE	RMSE	MAPE/%	R ²
<i>db4</i>	0.4454	0.5650	2.25	0.9027
<i>sym3</i>	0.7859	1.1275	4.35	0.7921
<i>haar</i>	0.2146	0.2573	1.09	0.9840
<i>coif3</i>	0.3689	0.6025	1.79	0.9121

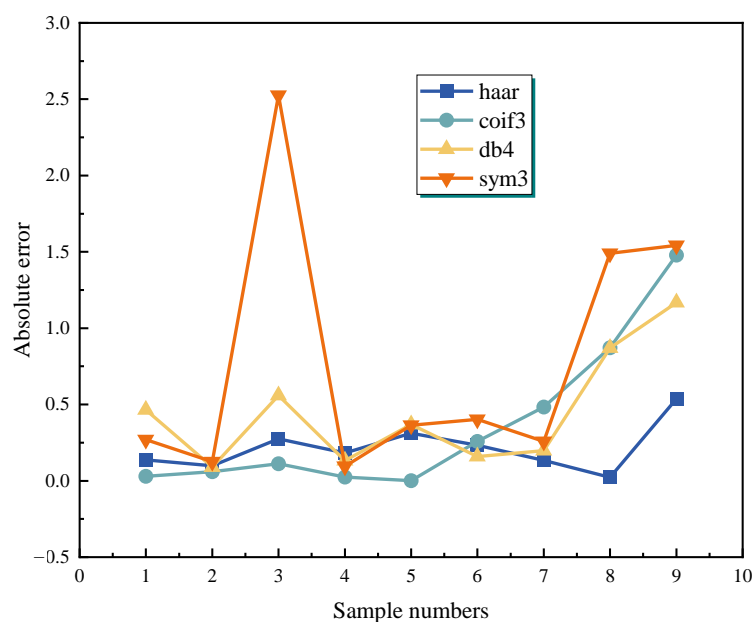


Figure 11. Absolute error comparison of prediction by DELM.

This section presents a detailed description of the experimental results using the complete full-scale data for deep extreme learning machine prediction. It further confirms the effectiveness of the wavelet feature parameters obtained through MSA for TGO thickness inversion and highlights the superiority of the *haar* wavelet basis function for prediction. This research contributes to a more comprehensive understanding of TGO thickness variations through inversion analysis.

Based on the study conducted, a multi-scale analysis was employed to extract wavelet coefficients from THz-TDS data using CWT. The extracted coefficients were further subjected to maximum pooling and utilized for the inversion of TGO thickness. Additionally, both multi-linear regression and machine learning regression models were employed to predict the TGO thickness, with TGO thickness as the dependent variable and wavelet feature parameters as the independent variables. The experimental results show that the wavelet feature parameters effectively represented the variations in TGO thickness, demonstrating high predictive accuracy. Particularly, the *haar* wavelet function exhibited the best predictive performance in both multi-linear regression and machine learning regression models. These findings highlight the exceptional performance of the *haar* wavelet function in multi-scale analysis, establishing it as a preferred choice for the optimal wavelet basis.

The findings of this research hold significant implications for the application of THz-TDS. The extraction of wavelet feature parameters through MSA enabled accurate prediction of TGO thickness, providing an effective approach for the detection and characterization of TGO in TBCs. Furthermore, by comparing multi-linear regression and machine learning regression models, the advantages of machine learning methods in TGO thickness prediction were demonstrated, further expanding the application scope of MSA. In

conclusion, the outstanding performance of multi-scale analysis on terahertz time-domain data and the effective characterization of TGO thickness using wavelet feature parameters establish the feasibility of precise TGO thickness inversion.

4. Conclusions

This study focuses on employing THz-TDS with a multi-scale analysis approach to estimate the TGO thickness in TBCs. Specifically, THz-TDS were obtained from FDTD simulations for different TGO thicknesses (30 sets). The MSA technique was used to extract features by applying continuous wavelet transformation with four wavelet basis functions (db4, sym3, haar, coif3). The max-pooling method was utilized to derive feature parameters from the wavelet coefficients. Visualization of the correlation between feature parameters and TGO thickness revealed a clear pattern, where the dimensionless value of feature parameters decreased as TGO thickness increased. Additionally, the feature parameter curve exhibited an increasing then decreasing trend with an increasing scale, displaying a noticeable peak. Smaller scales effectively captured low-frequency details, whereas larger scales had a weaker correlation with high-frequency features and TGO thickness. Multi-linear regression and machine learning regression models were used with wavelet feature parameters as inputs (the 21st–40th scales for multi-linear regression and full-scale data for DELM) and TGO thickness as output. Multi-linear regression considered the issue of rank deficiency, while machine learning was suitable for large datasets and sample sizes; both methods successfully performed the inversion, demonstrating the strong correlation and robustness between the multi-scale data and thickness. Experimental results revealed that the regression coefficients for the haar wavelet achieved the highest prediction accuracies of 0.9763 and 0.9840 for the two models, respectively, further validating the effectiveness of wavelet feature parameters obtained through multi-scale analysis for TGO thickness inversion.

In summary, this study accomplished the inversion of TGO thickness using multi-scale analysis techniques. It demonstrated the effectiveness of wavelet feature parameters derived from the multi-scale analysis in TGO thickness inversion and validated the haar wavelet as the optimal choice for the wavelet basis function. It is vital to acknowledge the limitations of this research and identify future directions for improvement. The study employed a relatively small sample size, and its applicability to larger datasets requires further validation. Moreover, additional research and optimization are needed for the selection of wavelet basis functions, parameter tuning, and exploration of other machine learning algorithms. Additionally, the integration of other feature extraction methods and prediction models could enhance the stability and robustness of the predictions. This study provided valuable references for the problem of TGO thickness inversion, offering a reliable methodology and theoretical basis for TGO thickness inversion. The practical implications of this research are related its applicability to practical scientific investigations and non-destructive testing in the realm of thermal barrier coatings.

Author Contributions: Conceptualization, D.Y. and J.X.; Data curation, J.X.; Funding acquisition, D.Y. and J.P.; Investigation, R.L., D.Y. and J.X.; Methodology, R.L. and J.X.; Project administration, J.P.; Resources, J.P.; Software, R.L.; Supervision, D.Y.; Validation, R.L.; Visualization, D.Y.; Writing—original draft, R.L. and D.Y.; Writing—review & editing, R.L. and J.P. All authors have read and agreed to the published version of the manuscript.

Funding: This research was funded by the National Natural Science Foundation of China (52205547), Key Research and Development Projects in Anhui Province (2022a05020004, 202104a05020002), Open Research Fund of Fujian Provincial Key Laboratory of Terahertz Functional Devices and Intelligent Sensing, Fuzhou University (FPKLTFDIS202301), Open Research Fund of Huzhou Key Laboratory of Terahertz Integrated Circuits and Systems (HKLTCY23KFO5), Open Research Fund of Anhui Key Laboratory of Detection Technology and Energy Saving Devices (JCKJ2022A08), Anhui Institute of Future Technology Enterprise Cooperation Project (2023qyh04), Scientific Research Starting Foundation of Anhui Polytechnic University (2021YQQ029).

Institutional Review Board Statement: Not applicable.

Informed Consent Statement: Not applicable.

Data Availability Statement: Not applicable.

Conflicts of Interest: The authors declare no conflict of interest.

References

1. Sohret, Y. Defining ecologic thermo-environmental index for aero-engines as a novel performance criterion. *Propul. Power Res.* **2021**, *10*, 374–382.
2. Liu, Q.; Huang, S.; He, A. Composite ceramics thermal barrier coatings of yttria stabilized zirconia for aero-engines. *J. Mater. Sci. Technol.* **2019**, *35*, 2814–2823.
3. Wang, K.; Peng, H.; Guo, H.; Gong, S. Effect of sintering on thermal conductivity and thermal barrier effects of thermal barrier coatings. *Chin. J. Aeronaut.* **2012**, *25*, 511–816. [[CrossRef](#)]
4. An, G.; Li, W.; Feng, L.; Cheng, B.; Wang, Z.; Li, Z.; Zhang, Y. Isothermal oxidation and TGO growth behaviors of YAG/YSZ double-ceramic-layer thermal barrier coatings. *Ceram. Int.* **2021**, *47*, 24320–24330.
5. Doleker, K.; Karaoglanli, A. Comparison of oxidation behavior of YSZ and Gd₂Zr₂O₇ thermal barrier coatings (TBCs). *Surf. Coat. Technol.* **2016**, *318*, 198–207. [[CrossRef](#)]
6. Shi, J.; Zhang, T.; Sun, B.; Wang, B.; Zhang, X.; Song, L. Isothermal oxidation and TGO growth behavior of NiCoCrAlY-YSZ thermal barrier coatings on a Ni-based superalloy. *J. Alloys Compd.* **2020**, *844*, 156093.
7. Torkashvand, K.; Poursaeidi, E.; Mohammadi, M. Effect of TGO thickness on the thermal barrier coatings life under thermal shock and thermal cycle loading. *Ceram. Int.* **2018**, *44*, 9283–9293. [[CrossRef](#)]
8. Feng, Y.; Dong, T.; Li, G.; Wang, R.; Zhao, X.; Liu, Q. High temperature oxidation resistance and TGO growth mechanism of laser remelted thermal barrier coatings. *J. Alloys Compd.* **2020**, *828*, 154266.
9. Ouyang, T.; Wu, J.; Yasir, M.; Zhou, T.; Fang, X.; Wang, Y.; Liu, D.; Suo, J. Effect of TiC self-healing coatings on the cyclic oxidation resistance and lifetime of thermal barrier coatings. *J. Alloys Compd.* **2016**, *656*, 992–1003.
10. Li, B.; Fan, X.; Zhou, K.; Wang, T. Effect of oxide growth on the stress development in double-ceramic-layer thermal barrier coatings. *Ceram. Int.* **2017**, *43*, 14763–14774. [[CrossRef](#)]
11. Song, X.; Meng, F.; Kong, M.; Wang, Y.; Huang, L.; Zheng, X.; Zeng, Y. Thickness and microstructure characterization of TGO in thermal barrier coatings by 3D reconstruction. *Mater. Charact.* **2016**, *120*, 244–248. [[CrossRef](#)]
12. Huang, H.; Liu, C.; Ni, L.; Zhou, C. Evaluation of TGO growth in thermal barrier coatings using impedance spectroscopy. *Rare Met.* **2011**, *30*, 643–646. [[CrossRef](#)]
13. Ma, Z.; Zhao, Y.; Luo, Z.; Lin, L. Ultrasonic characterization of thermally grown oxide in thermal barrier coating by reflection coefficient amplitude spectrum. *Ultrasonics* **2014**, *54*, 1005–1009. [[CrossRef](#)]
14. Zhang, X.; Zhao, Y.; Withers, P.; Xiao, P. Microstructural degradation of electron beam-physical vapour deposition thermal barrier coating during thermal cycling tracked by X-ray micro-computed tomography. *Scr. Mater.* **2018**, *152*, 79–83. [[CrossRef](#)]
15. Sun, F.; Fan, M.; Cao, B.; Ye, B.; Liu, L. High-resolution terahertz imaging of de-bonding defects in thermal barrier coatings using an optimal wavelet transform. *IEEE Trans. Instrum. Meas.* **2023**, 3293872. [[CrossRef](#)]
16. Sun, F.; Fan, M.; Cao, B.; Liu, L. THzResNet: A physics-inspired two-stream residual network for thermal barrier coating thickness measurement. *IEEE Trans. Ind. Inform.* **2022**, *19*, 8328–8339. [[CrossRef](#)]
17. Ye, D.; Wang, W.; Zhou, H.; Fang, H.; Huang, J.; Li, Y.; Gong, H.; Li, Z. Characterization of thermal barrier coatings microstructural features using terahertz spectroscopy. *Surf. Coat. Technol.* **2020**, *394*, 125836. [[CrossRef](#)]
18. Ye, D.; Wang, W.; Zhou, H.; Li, Y.; Fang, H.; Huang, J.; Gong, H.; Li, Z. Quantitative determination of porosity in thermal barrier coatings using terahertz reflectance spectrum: Case study of atmospheric-plasma-sprayed YSZ coatings. *IEEE Trans. Terahertz Sci. Technol.* **2020**, *10*, 383–390. [[CrossRef](#)]
19. Ye, D.; Wang, W.; Zhou, H.; Huang, J.; Wu, W.; Gong, H.; Li, Z. In-situ evaluation of porosity in thermal barrier coatings based on the broadening of terahertz time-domain pulses: Simulation and experimental investigations. *Opt. Express* **2019**, *27*, 28150–28165. [[CrossRef](#)]
20. Chen, C.; Lee, D.; Pollock, T.; Whitaker, J. Terahertz characterization of interfacial oxide layers and voids for health monitoring of ceramic coatings. In Proceedings of the 2009 34th International Conference on Infrared, Millimeter, and Terahertz Waves, Busan, Republic of Korea, 21–25 September 2009.
21. Zhang, Z.; Huang, Y.; Zhong, S.; Lin, T.; Zhong, Y.; Zeng, Q.; Nsengiyumva, W.; Yu, Y.; Peng, Z. Time of flight improved thermally grown oxide thickness measurement with terahertz spectroscopy. *Front. Mech. Eng.* **2022**, *17*, 49. [[CrossRef](#)]
22. Luo, M.; Zhong, S.; Yao, L.; Tu, W.; Nsengiyumva, W.; Chen, W. Thin thermally grown oxide thickness detection in thermal barrier coatings based on SWT-BP neural network algorithm and terahertz technology. *Appl. Opt.* **2020**, *59*, 4097–4104. [[CrossRef](#)] [[PubMed](#)]
23. Stoik, C.; Bohn, M.; Blackshire, J. Nondestructive evaluation of aircraft composites using transmissive terahertz time domain spectroscopy. *Opt. Express* **2008**, *16*, 17039–17051. [[CrossRef](#)] [[PubMed](#)]

24. Zhang, R.; He, Y.; Liu, K.; Zhang, L.; Zhang, S.; Pickwell-MacPherson, E.; Zhao, Y.; Zhang, C. Composite multiscale entropy analysis of reflective terahertz signals for biological tissues. *Opt. Express* **2017**, *25*, 23669–23676. [[CrossRef](#)]
25. Yin, Y.; Shang, P. Detection of multiscale properties of financial market dynamics based on an entropic segmentation method. *Nonlinear Dyn.* **2016**, *83*, 1743–1756. [[CrossRef](#)]
26. Zhang, Z.; Gao, J.; Yang, M.; Yan, X.; Lu, Y.; Wu, L.; Li, J.; Wei, D.; Liu, L.; Xie, J.; et al. Microfluidic integrated metamaterials for active terahertz photonics. *Photonics Res.* **2019**, *7*, 1400–1406. [[CrossRef](#)]
27. Kozhanova, E.; Danilov, S.; Belyaev, V. Methods of recognition based on wavelet transform for analysis of characteristics of spherical quantum dot. *Eng. Proc.* **2023**, *33*, 35.
28. Zheng, Y.; Iwana, B.; Uchida, S. Mining the displacement of max-pooling for text recognition. *Pattern Recognit.* **2019**, *93*, 558–569. [[CrossRef](#)]
29. Mehmet, K. A study over the general formula of regression sum of squares in multiple linear regression. *Numer. Methods Partial. Differ. Equ.* **2020**, *37*, 406–421.
30. Jiang, X.; Yan, T.; Zhu, J.; He, B.; Li, W.; Du, H.; Sun, S. Densely connected deep extreme learning machine algorithm. *Cogn. Comput.* **2020**, *12*, 979–990. [[CrossRef](#)]
31. Sun, F.; Cao, B.; Fan, M.; Liu, L. Physics-based deep learning framework for terahertz thickness measurement of thermal barrier coatings. *SSRN Electron. J.* **2023**, 4373227. [[CrossRef](#)]

Disclaimer/Publisher’s Note: The statements, opinions and data contained in all publications are solely those of the individual author(s) and contributor(s) and not of MDPI and/or the editor(s). MDPI and/or the editor(s) disclaim responsibility for any injury to people or property resulting from any ideas, methods, instructions or products referred to in the content.